# Pressure evolution of $LiBaF_3:Eu^{2+}$ luminescence



2009 J. Phys.: Condens. Matter 21 235603

(http://iopscience.iop.org/0953-8984/21/23/235603)

J. Phys.: Condens. Matter **21** (2009) 235603 (8pp) doi:10.1088/0953-8984/21/23/235603

# Pressure evolution of $LiBaF_3:Eu^{2+}$ luminescence

**S Mahlik[1], M Grinberg[1], Liang Shi[2] and Hyo Jin Seo[2]**

[1] Institute of Experimental Physics, University of Gdansk, Wita Stwosza 57, 80-952 Gdansk, Poland
[2] Department of Physics, Pukyong National University, Busan 608-737, Republic of Korea

Received 4 February 2009, in final form 3 April 2009
Published 15 May 2009
Online at stacks.iop.org/JPhysCM/21/235603

**Abstract**

We investigated the single crystals of $LiBaF_3$ doped with $Eu^{2+}$ using high pressure spectroscopy, where high pressure was applied in a diamond anvil cell. Photoluminescence, time-resolved luminescence and luminescence kinetics at pressures from ambient to 200 kbar and at temperatures from 10 K to ambient were studied. At ambient conditions the luminescence spectra consisted of sharp lines peaked at 360 nm attributed to the $^6P_{7/2} \rightarrow {}^8S_{7/2}$ transitions in the $4f^7$ electronic configuration of $Eu^{2+}$ (the zero-phonon line and five single-phonon repetitions) and a broad band extending between 375 and 475 nm attributed to $Eu^{2+}$ trapped exciton recombination. When pressure was increased the $Eu^{2+}$ trapped exciton emission disappears and was replaced by the sharper band peaked at 355 nm, attributed to the $4f^65d^1(e_g) \rightarrow 4f^7(^8S_{7/2})$ transition in $Eu^{2+}$. To analyze the pressure dependence of luminescence spectra a model of impurity trapped excitons was developed. At temperatures lower than 50 K only the sharp lines related to $^6P_{7/2} \rightarrow {}^8S_{7/2}$ transitions were observed for all pressures considered. Analysis of low temperature spectra allowed us to estimate the energies of the fifth phonon modes and the values of the Grüneisen parameters.

## 1. Introduction

The complex fluoride $LiBaF_3$, both pure and doped with europium and cerium, have been investigated for 40 years due to their properties such as piezoelectric (Eibshultz *et al* 1969), ferroelectric (Cooke *et al* 1975) and nonmagnetic insulator (Heaton and Lin 1982) behavior. The broad band emission related to d–f transitions in dopants has been considered as a possible source of tunable laser radiation (Ehrilich *et al* 1979) and optical amplification (Sarakura 1995).

$LiBaF_3$ is a typical $ABX_3$ material (herein A—alkali ion, B—alkali-earth ion, X—halide ion) which has an inverse-perovskite with cubic structure ($a_0 = 3.988$ Å) (Baldochi and Gesland 1992). The $Li^+$ ion is surrounded by six $F^{1-}$ ions while the $Ba^{2+}$ ion is surrounded by twelve $F^{1-}$ ions. The regular lattice site of the $Ba^{2+}$ ion with twelvefold coordination in $LiBaF_3$ has the $O_h$ point group symmetry (Marsman *et al* 2000). In $LiBaF_3$, the doped $Eu^{2+}$ ions substitute the site of $Ba^{2+}$ ions.

The ground state of the $Eu^{2+}$ in $LiBaF_3$ is $^8S_{7/2}$ whereas the first excited state is the $^6P_{7/2}$ state, both belonging to the $4f^7$ electronic configuration. Energies of the states of excited electronic configuration $4f^65d^1(e_g)$ and $4f^65d^1(t_{2g})$ are higher. Luminescence of $LiBaF_3$ doped with $Eu^{2+}$ has been studied in several papers (Aldshuler *et al* 1974, Sommerdijk *et al* 1974, Tunguy *et al* 1974, Meijerink 1993, Hua *et al* 2003, Zhou *et al* 2002). It has been found that the emission spectrum consists of a broad band ranging from 370 to 500 nm and sharp lines located at 360 nm. The sharp lines have been attributed to the $^6P_{7/2} \rightarrow {}^8S_{7/2}$ transitions in the $4f^7$ electronic configuration of $Eu^{2+}$, whereas the broad band was related to the $4f^65d^1(e_g) \rightarrow 4f^7(^8S_{7/2})$ transition in $Eu^{2+}$ (Meijerink 1993, Zhou *et al* 2002) or to traces of oxygen in the powder materials (Hua *et al* 2003).

In this paper we present detailed spectroscopic investigations of the $LiBaF_3:Eu^{2+}$ crystals that obey photoluminescence, time-resolved spectroscopy and luminescence kinetics experiments. To analyze the energetic structure of the system and the origins of the individual luminescence features we performed experiments at different temperatures and under different high hydrostatic pressures. The main purpose of our research was to understand the nature of the broad band emission.

 

## 2. Experimental procedures

### *2.1. Crystal growth of $LiBaF_3$ single crystals*

Single crystals of $LiBaF_3$ doped with $Eu^{2+}$ ions were grown from the melt in Ar-gas atmosphere by the Czochralski method. The starting materials were prepared by the high temperature solid state reaction method. The molar ratio of LiF and $BaF_2$ was 3:2. The powders were dried for 10–20 h at 300 °C and heated up to 650 °C at a rate of 2 °C $min^{-1}$ in a vacuum chamber. After annealing at 650 °C for 10 h the temperature was increased to the melting point at around 790 °C in a furnace filled with Ar gas with a chamber pressure of 1.5 atm. The pulling speed was 5 mm $h^{-1}$ and the rotation was 10 rpm. Single crystals up to 5 cm in length and 2 cm in diameter were successfully pulled and were then slowly cooled to room temperature.

### *2.2. Steady state luminescence*

Steady state luminescence was excited with an He–Cd laser at a wavelength of 325 nm. Luminescence was dispersed by a PGS2 spectrometer working as a monochromator and detected by an R943-2 photomultiplier working in the photon counting regime. Luminescence excitation spectra were measured using a system consisting of an Xe lamp (450 W), two monochromators SPM2 (one in the excitation and one in the detection line) and two photomultipliers (the first for the luminescence and the second for reference signal detection). The absorption spectrum has been measured using an M 40 SPECORD standard spectrometer.

### *2.3. Time-resolved luminescence*

To obtain the time dependence of the emission, samples were excited with an optical parametric generator PG401/SH pumped by the tripled output of a pulsed Nd:YAG laser. The luminescence kinetics was measured at room temperature using a Hamamatsu C4334-01 model Streak Camera. The luminescence was spectrally separated with a Bruker Optics 2501S model monochromator. Details of the set-up are presented in the paper Kubicki *et al* (2006).

### *2.4. High pressure technique*

High pressure experiments were performed in a diamond anvil cell (DAC). The sample was placed in a hole drilled in a inconel x750 steel gasket between two parallel diamond anvils. Pressure appears when the diamonds are moved and is transmitted to the fluid medium. A ruby crystal was used as the pressure detector. We estimated pressure with an accuracy of about 2 kbar. Dow Corning Corporation 200 fluid was used as the pressure transmitting medium.

## 3. Experimental results

In figure 1 the absorption, luminescence and excitation spectra of $LiBaF_3$:$Eu^{2+}$ obtained at ambient conditions are presented. Emission obtained under excitation at 325 nm is presented by a dotted curve and consists of sharp lines in the spectral range 27 500–28 000 $cm^{-1}$ related to internal transitions from $^6P_{7/2} \rightarrow {}^8S_{7/2}$ in the $Eu^{2+}$. The detailed structure of these lines is presented in figure 2(a), where the luminescence measured for different temperatures is presented. Apart from these sharp lines the broad band emission peaked at 24 500 $cm^{-1}$ was seen. Actually this band was structureless and the structure seen in figure 1 is related to absorption by the interferometric filter that was used for dumping the laser excitation light. The broad band emission has been earlier attributed to emission from the excited electronic manifold of $Eu^{2+}$, $4f^65d^1(e_g)$ (Meijerink 1993). In this paper we attributed this band to recombination of the $Eu^{2+}$ trapped exciton. We considered that this luminescence had the same origin as the anomalous luminescence in the $BaF_2$:$Eu^{3+}$ lattice (Gatch *et al* 2006), (Mahlik *et al* 2008), and other crystals doped with $Eu^{2+}$ and $Yb^{2+}$ (Dorenbos 2003b).

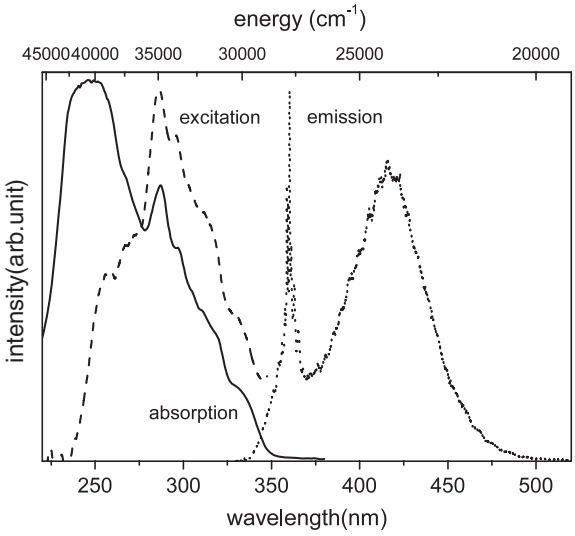


**Figure 1.** Absorption (solid curve), luminescence (dashed–dotted) and luminescence excitation (dashed) spectra of $LiBaF_3$:$Eu^{2+}$ obtained at ambient pressure at room temperature.

The luminescence excitation spectrum is presented by the dashed curve. The excitation spectrum has the same shape independent of the $^6P_{7/2} \rightarrow {}^8S_{7/2}$ or broad band luminescence was monitored. The absorption spectrum is presented by the solid curve. The structure in the absorption and excitation spectrum with peaks in the range 28 600 to 40 000 $cm^{-1}$ has been related to spin-allowed transitions from the ground state $^8S_{7/2}$ to the states of the excited electronic configuration $4f^65d^1$ of $Eu^{2+}$ (Dorenbos 2003a).

Ambient pressure luminescence spectra of $LiBaF_3$:$Eu^{2+}$ obtained at different temperatures are presented in figures 2(a) and (b). One considers the structure of the $^6P_{7/2} \rightarrow {}^8S_{7/2}$ transition seen in figure 2(a). It consists of several sharp lines: the line peaked at 27 850 $cm^{-1}$ was related to the zero-phonon transition and five bands with lower energies labeled $\nu_1$, $\nu_2$, $\nu_3$, $\nu_4$ and $\nu_5$ seen at all temperatures were related to the one-phonon repetition of the zero-phonon line. Energies of the bands obtained at 10 K are listed in table 1. The energies of phonons were in accordance with those obtained

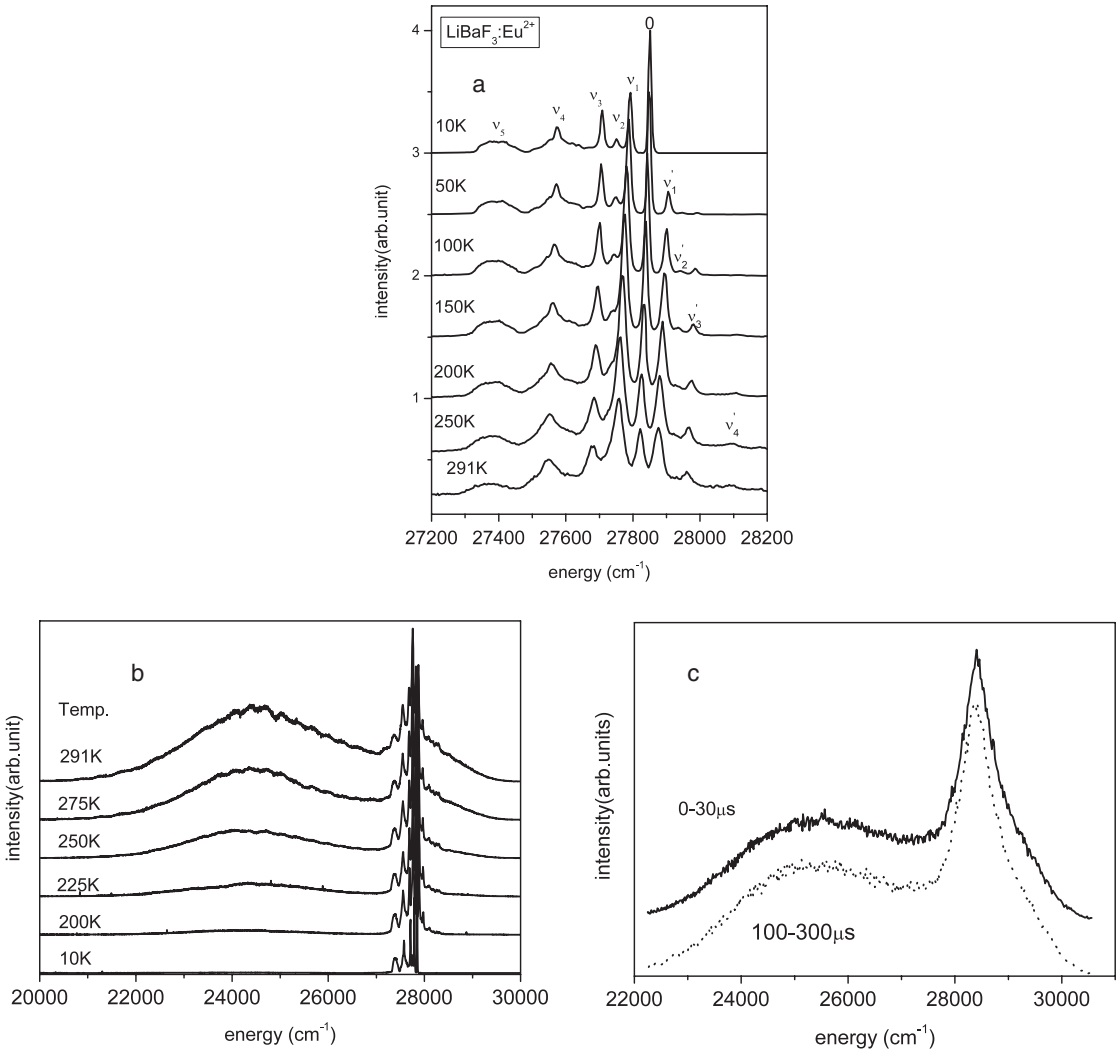


**Figure 2.** Ambient pressure luminescence spectra of $LiBaF_3:Eu^{2+}$ obtained at different temperatures: (a) the structure of the $^6P_{7/2} \rightarrow {}^8S_{7/2}$ transition, (b) whole spectra and (c) room temperature time-resolved spectra. For details see the text.

earlier (Meijerink 1993). Since we found neither the IR or Raman spectra of $LiBaF_3$ the phonons were not assigned to specific vibration modes. The energies of vibrations 1, 2 and 3 were estimated from the position of the energy peaks at 10 K with an accuracy $\pm 1$ cm$^{-1}$. Two remaining lines were broader and energies $h\nu_4 = 275$ cm$^{-1}$ and $h\nu_5 = 450$ cm$^{-1}$ represented the maxima of the respective phonon bands. At higher temperatures in the anti-Stokes part of the vibronic spectra the lines labeled as $\nu_1'$, $\nu_2'$, $\nu_3'$ and $\nu_4'$ were seen, which corresponded to the respective lines in the Stokes spectrum. The zero-phonon transition shifted to the red region with temperature at the rate $-0.11$ cm$^{-1}$ K$^{-1}$. Only the phonon energy $h\nu_1$ depended on temperature. We found that $\mathrm{d}(h\nu_1)/\mathrm{d}T = 0.02 \pm 0.002$ cm$^{-1}$ K$^{-1}$.

In figure 2(b) it is seen that at temperatures lower than 150 K only the $^6P_{7/2} \rightarrow {}^8S_{7/2}$ sharp emission is observed. With increasing temperature the contribution of the broad band luminescence increased. Apart from the excitonic, an additional broad band peaked at about 28 000 cm$^{-1}$ appeared. This band was related to the $4f^65d^1(e_{2g}) \rightarrow {}^8S_{7/2}$ transition in $Eu^{2+}$.

**Table 1.** Phonon energies and values of the Grüneisen parameter ($B = 743$ kbar (Haussühl *et al* 1972)).

| | $h\nu$ (cm$^{-1}$) | $\frac{\mathrm{d}h\nu}{\mathrm{d}p}$ (cm$^{-1}$ kbar$^{-1}$) | $\gamma = \frac{B}{\nu}\frac{\mathrm{d}\nu}{\mathrm{d}p}$ |
|---|---|---|---|
| $\nu_1$ | $58 \pm 1$ | $0.25 \pm 0.01$ | 3.20 |
| $\nu_2$ | $99 \pm 1$ | | |
| $\nu_3$ | $142 \pm 1$ | $0.32 \pm 0.01$ | 1.02 |
| $\nu_4$ | $\approx 275$ | $0.33 \pm 0.02$ | 0.89 |
| $\nu_5$ | $\approx 450$ | $0.56 \pm 0.03$ | 0.92 |

We measured the time-resolved luminescence at ambient temperature. The results are presented in figure 2(c). The solid curve represents the luminescence measured in the time interval 0–30 $\mu$s whereas the dotted curve represents the emission measured in the time interval 100–300 $\mu$s, after excitation. We found that the spectral lineshape did not change with time. The luminescence decayed exponentially, all features at the same time. Therefore we considered that occupations of the $^6P_{7/2}$ state, $4f^65d^1$ state and $Eu^{2+}$ trapped exciton state were in thermal equilibrium. At ambient pressure

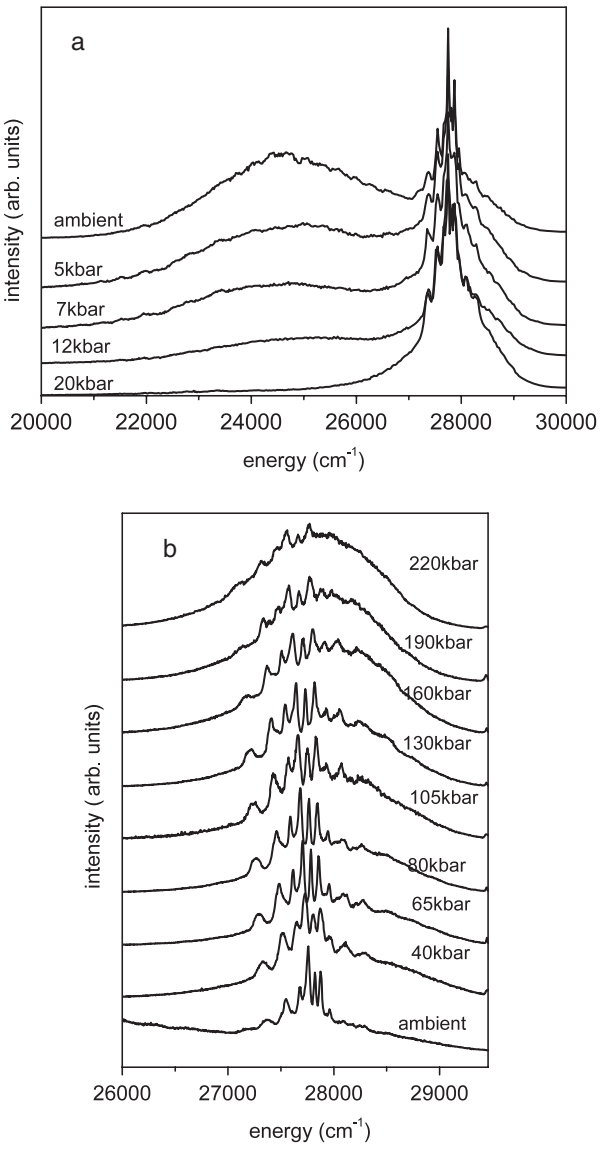


**Figure 3.** Luminescence spectra of $LiBaF_3:Eu^{2+}$ obtained at different pressures at ambient temperature: (a) whole spectra and (b) the region of the $^6P_{7/2} \rightarrow {}^8S_{7/2}$ emission. The spectra are normalized with respect to the maximum intensity of the $^6P_{7/2} \rightarrow {}^8S_{7/2}$ emission.

the first excited state was the $^6P_{7/2}$ state of $Eu^{2+}$ and the next excited states were the $Eu^{2+}$ trapped exciton state and the $4f^65d^1(e_g)$ state. The detailed discussion of the energetic structure of the $LiBaF_3:Eu^{2+}$ is presented in the next section.

In figures 3(a) and (b) the luminescence obtained at different pressures at ambient temperature are presented. The spectra are normalized with respect to the maximum intensity of the $^6P_{7/2} \rightarrow {}^8S_{7/2}$ emission. One noticed that the contribution from the impurity trapped exciton (the broad band peaked at 24 500 $cm^{-1}$) diminished with increased pressure and vanished for a pressure of 20 kbar (see figure 3(a)). This effect was attributed to an increase of the energy of the $Eu^{2+}$ trapped exciton state with respect to the $^6P_{7/2}$ state of $Eu^{2+}$, $\Delta_{ef}$, when pressure increases. Considering figure 3(a) one noticed that reduction of the intensity of excitonic emission was not accompanied by their shift towards higher energy. For pressures between 20 and 40 kbar the $^6P_{7/2} \rightarrow {}^8S_{7/2}$ emission dominated at the ambient temperature spectra. At pressures above 40 kbar an additional broad band luminescence peaked at about 28 000 $cm^{-1}$ started to dominate the spectrum (see figure 3(b)). This emission was attributed to the transition from the $4f^65d^1(e_g)$ state to the ground state $^8S_{7/2}$ of $Eu^{2+}$.

We measured pressure dependence of the luminescence related to the $^6P_{7/2} \rightarrow {}^8S_{7/2}$ transition. In figure 4(a) luminescence related to the $^6P_{7/2} \rightarrow {}^8S_{7/2}$ emission obtained at 10 K at different pressures is presented. The dashed curve represents the ambient pressure spectrum of a macroscopic sample (outside the DAC) obtained at 10 K. One noticed that the spectrum of the microscopic sample consisted of broader lines. This was the apparatus effect related to a broader slot needed for detection of the luminescence of microscopic samples. We observed the pressure redshifts of all lines. We estimated the pressure shift of the energy of the zero-phonon line as $-0.95 \pm 0.01$ $cm^{-1}$ $kbar^{-1}$. The shifts of the phonon lines were stronger as the result of the increase of energies of the phonon modes with increasing pressure. Obtained data are listed in table 1. The increase in energies of the phonon modes with increasing pressure was related to the increase in crystal stiffness and bulk modulus. One calculated the values of the Grüneisen parameter (see table 1) which were of the order of unity and only for phonon $\nu_1$ was the Grüneisen parameter equal to 3.2.

We measured the temperature dependence of the luminescence at a pressure of 200 kbar. The results are presented in figure 4(b). For temperature below 150 K only the $^6P_{7/2} \rightarrow {}^8S_{7/2}$ emission was observed. For temperatures above 200 K the intensity of the broad band related to the $4f^65d^1(e_g) \rightarrow {}^8S_{7/2}$ transition rose rapidly and at room temperature it dominated the spectrum. Such a dependence was attributed to the fact that, for a pressure of 200 kbar the $4f^65d^1$ state was the second excited state.

The results presented in figure 3(b) showed that the difference between the energy of the $4f^65d^1(e_g)$ state and the $^6P_{7/2}$ state, $\Delta_{df}$, was reduced with increasing pressure. This effect was well seen when one compared the spectra obtained at the same temperature for different pressures. The respective spectra measured at 170 and 200 kbar are presented in figure 4(c). One noticed that for 200 kbar the $4f^65d^1(e_g) \rightarrow {}^8S_{7/2}$ transition started to dominate the emission at 200 K, whereas for 170 kbar it happened at 275 K, thus the energy $\Delta_{df}$ was smaller for 200 kbar than for 170 kbar. On the other hand, it was quite surprising that the reduction of energy $\Delta_{df}$ was not correlated to a reduction of the energy of the $4f^65d^1(e_g) \rightarrow {}^8S_{7/2}$ transition. Actually even a small blue shift of the $4f^65d^1(e_g) \rightarrow {}^8S_{7/2}$ luminescence was observed (see figure 4(c)).

We measured the time-resolved luminescence spectra and luminescence kinetics. Obtained results were in accordance with the steady state luminescence data.

Decays of the luminescence related to recombination of the $Eu^{2+}$ trapped exciton monitored between 23 000 and 25 000 $cm^{-1}$ obtained at ambient and at 8 kbar are presented in figure 5. One noticed that the luminescence decayed

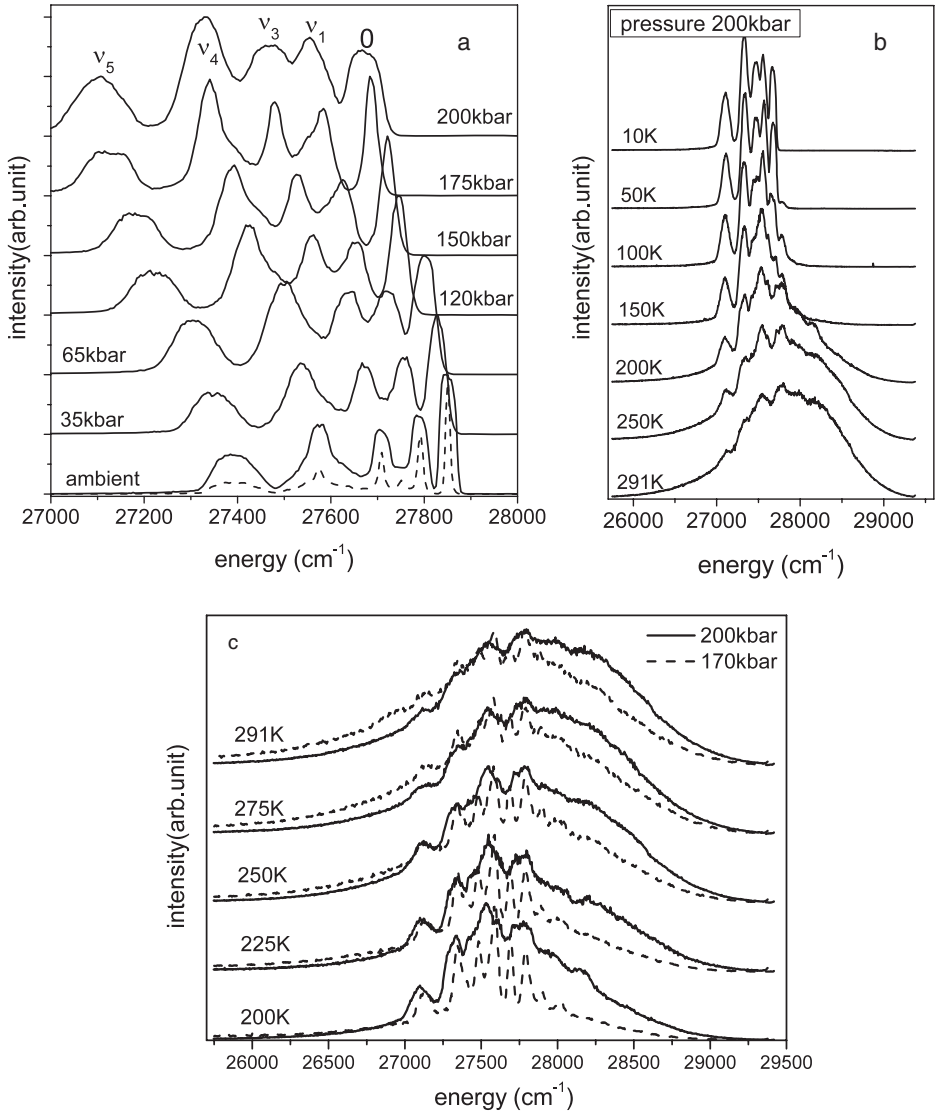


**Figure 4.** Luminescence spectra of $LiBaF_3:Eu^{2+}$. (a) The $^6P_{7/2} \rightarrow {}^8S_{7/2}$ emission at 10 K at different pressures for microscopic samples in DAC. Dashed curve presents the spectrum obtained for macroscopic samples without DAC. (b) Luminescence spectra of $LiBaF_3:Eu^{2+}$ at 200 kbar at different temperatures. (c) Luminescence spectra of $LiBaF_3:Eu^{2+}$ at 200 and 170 kbar at different temperatures.

exponentially with the lifetimes 84 $\mu$s and 130 $\mu$s for ambient pressure and 8 kbar, respectively.

Decays of the emission spectra monitored in the spectral range between 27 000 and 29 000 $cm^{-1}$, which corresponded to the $^6P_{7/2} \rightarrow {}^8S_{7/2}$ emission and the $4f^65d^1(e_g) \rightarrow {}^8S_{7/2}$ obtained at different pressure at room temperature are presented in figures 6(a) and (b). The obtained luminescence lifetime increased from 84 $\mu$s at ambient pressure to 320 $\mu$s at 33 kbar (see figure 6(a)) and remained constant up to 70 kbar, and then for pressures greater than 70 kbar decreased with increasing pressure (see figure 6(b)). Actually for pressures higher than 120 kbar decay was not single-exponential and one has to define the effective lifetime $\hat{\tau} = \frac{\int I(t)t\,dt}{\int I(t)\,dt}$. We found that for a pressure of 200 kbar $\hat{\tau} = 57$ $\mu$s.

To consider the relations between energies of the $4f^65d^1(e_g)$ state, $^6P_{7/2}$ state and $Eu^{2+}$ trapped exciton state, and respective luminescence we used the model where the decay constant describing the luminescence decay of the multi-level system was given by the relation

$$\frac{1}{\tau} = \frac{1}{\tau_{ff}} + \frac{\exp\left(\frac{-\Delta_{ef}}{kT}\right)}{\tau_{ef}} + \frac{\exp\left(\frac{-\Delta_{df}}{kT}\right)}{\tau_{df}}. \qquad (1)$$

In relation (1) $\tau$, $\tau_{ff}$, $\tau_{ef}$ and $\tau_{df}$ are the effective radiative lifetimes and the radiative lifetimes of the $^6P_{7/2}$ state, $Eu^{2+}$ trapped exciton state and $4f^65d^1$ state, respectively. $\Delta_{ef}$ and $\Delta_{df}$ were the differences between the energy of the $^6P_{7/2}$ state of $Eu^{2+}$ and the $4f^65d^1(e_g)$ state and $^6P_{7/2}$ state, respectively.

The spectra at ambient pressure and at 8 kbar consisted of the $Eu^{2+}$ trapped exciton emission and the f–f emission of $Eu^{2+}$. Thus we neglected the third component of the sum (1) as not contributing to the luminescence. Considered that the $^6P_{7/2} \rightarrow {}^8S_{7/2}$ emission is forbidden with respect to the parity and spin we assumed that $\tau_{ff} \gg \tau_{ef}$. Thus increasing the effective luminescence lifetime with increasing pressure was

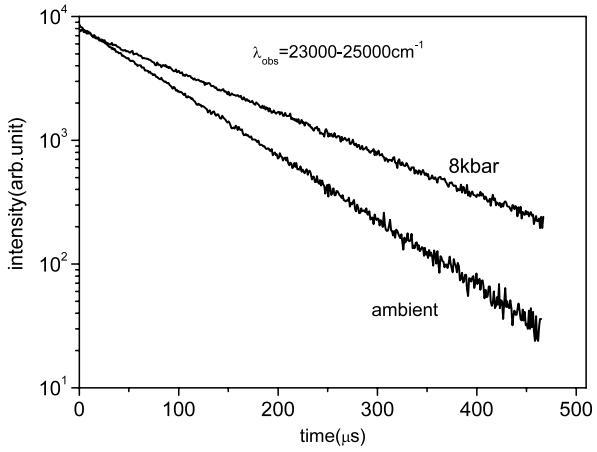


**Figure 5.** Decays of the luminescence related to recombination of $Eu^{2+}$ exciton monitored between 23 000 and 25 000 $cm^{-1}$ obtained at room temperature at ambient pressure and at 8 kbar are presented.

related to the increase of energy $\Delta_{ef}$. The increase of the luminescence lifetime with increasing pressure for the pressure range from ambient to 33 kbar, presented in figure 6(a), was also related to the increase in the energy of $\Delta_{ef}$. Further decrease of the luminescence lifetime for the pressure range 70–200 kbar, presented in figure 6(b), was also considered using relation (1). One shows that for this pressure range the $Eu^{2+}$ exciton trapped luminescence was not observed. Therefore we neglected the second component in relation (1) and the emission lifetime was controlled by quantities $\tau_{ef}$, $\tau_{df}$ and $\Delta_{df}$. Under the assumption that $\tau_{ff} > \tau_{df}$ relation (1) yielded that the decrease of the luminescence lifetime was caused by the decrease in energy $\Delta_{df}$.

## 4. Pressure dependence of f–f, d–f emission and $Eu^{2+}$ trapped exciton emission

To analyze the energetic structure of the $LiBaF_3:Eu^{2+}$ system and the dependence of the luminescence on pressure we proposed the configurational coordinate diagram presented in figure 7. Solid thin parabolas represent the energies of the ground state $^8S_{7/2}$ and the excited state $^6P_{7/2}$ of $Eu^{2+}$, the

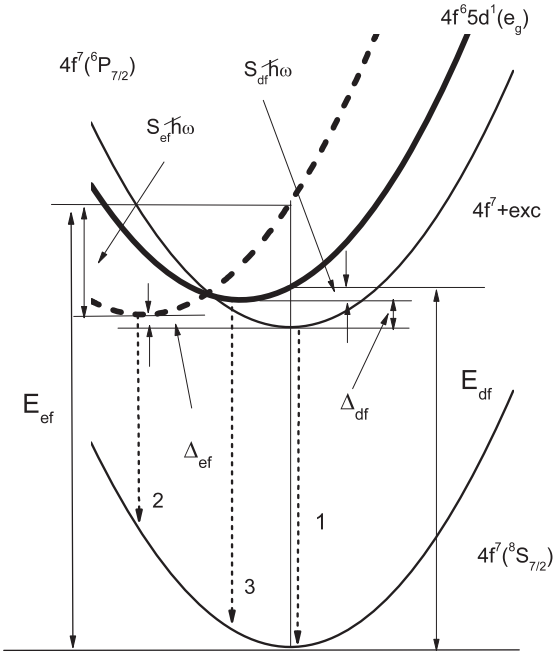


**Figure 7.** Configurational coordinate diagram representing the $LiBaF_3:Eu^{2+}$ system.

thick solid parabola shifted to the left represents the excited state $4f^65d^1(e_g)$ of the $Eu^{2+}$ ion and the dashed thick parabola represents the $Eu^{2+}$ trapped exciton. The vertical arrows labeled 1, 2 and 3 correspond to the $^6P_{7/2} \rightarrow {}^8S_{7/2}$, $Eu^{2+}$ trapped exciton recombination and the $4f^65d^1(e_g) \rightarrow {}^8S_{7/2}$ transition, respectively. The length of the arrows corresponds to energies of the transition peaks. One defined the electron–lattice coupling energies: $S_{df}\hbar\omega$ in the case of the system in the $4f^65d^1(e_g)$ and $S_{ef}\hbar\omega$ in the case of the $Eu^{2+}$ trapped exciton state, where $S_{df}$ and $S_{ef}$ are the respective Huang–Rhys factors and $\hbar\omega$ is the energy of the local phonon mode. Usually $S_{df}\hbar\omega \ll S_{ef}\hbar\omega$.

Due to the screening effect of the $5s^25p^6$ electrons the influence of ligands on electrons in the $4f^7$ shell of the $Eu^{2+}$ is small. As the result we observed only a small redshift of the $^6P_{7/2} \rightarrow {}^8S_{7/2}$ luminescence. A different situation is in

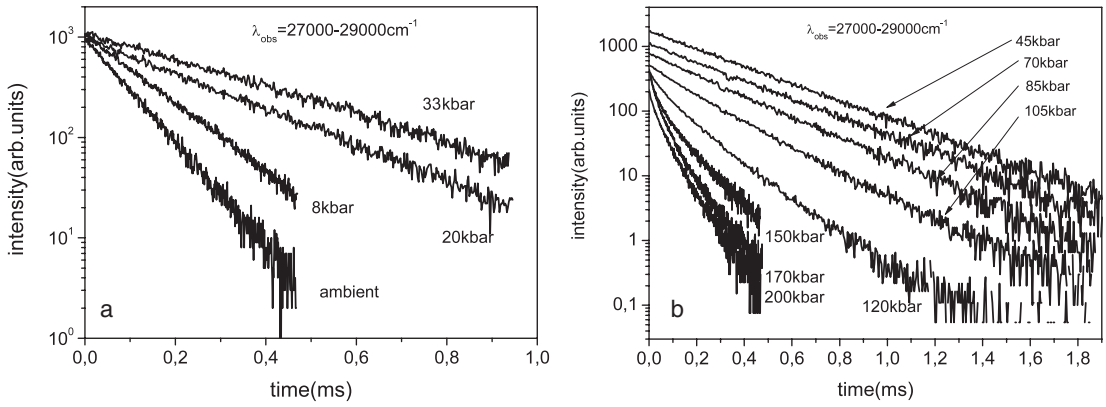


**Figure 6.** Decays of the emission spectra of $LiBaF_3:Eu^{2+}$ monitored for the spectral range between 27 000 and 29 000 $cm^{-1}$ obtained at different pressure at room temperature: (a) ambient–33 kbar; (b) 45–200 kbar.

the case of the $4f^6 5d^1(t_2) \rightarrow {}^8S_{7/2}$ transition. The excited electronic manifold $4f^6 5d^1$ was split by the crystal field into $4f^6 5d^1(e_g)$ and $4f^6 5d^1(t_{2g})$ states, where in the cubic crystal field the $4f^6 5d^1(e_g)$ state had lower energy. Since pressure compresses the crystal and the crystal field strength depends on the $Eu^{2+}$–ligand distance, energies of the $4f^6 5d^1(e_g)$ and $4f^6 5d^1(t_{2g})$ states are sensitive to pressure. The influence of pressure on the energy of the excited electronic manifold $4f^{n-1}5d^1$ has already been investigated in the case of $Ce^{3+}$ and $Pr^{3+}$ in oxide crystals (the last review one can find in Grinberg (2006)) and $Eu^{2+}$-doped oxides (Tyner and Drickamer 1977), fluorides (Gatch *et al* 2006, Mahlik *et al* 2008) and bromides (Tröster *et al* 2002). Assuming that the pressure effects are linear the energy of the lower state of the excited electronic configuration labeled by $E_{df}$ in figure 7 reduces with pressure at the rate (Grinberg 2006)

$$\frac{dE_{df}}{dp} = -\frac{nE_{depr}}{3B} \tag{2}$$

where $E_{depr}$ is the depression energy (Dorenbos 2000) which is related mainly to crystal field splitting of the $4f^6 5d^1$ state and the centroid shift describing the changes in ligand polarization (Morrison 1980), $n$ is the exponent that controls the dependence of these quantities on the central ion–ligand distance (usually one assumes $n \approx 5$) and $B$ is the bulk modulus.

Transition from the ground electronic configuration $4f^7$ to the excited electronic configuration $4f^6 5d^1$ causes the lattice relaxation. When the system is in the $4f^6 5d^1(e_g)$ state a small collapse of ligands with respect to their positions for the ground electronic configuration was expected. This effect causes a reduction of the energy of the system by $S_{df}\hbar\omega$. The linear effect of the dependence of pressure on $S_{df}\hbar\omega$ can be described by the rate (Grinberg 2006)

$$\frac{dS_{df}\hbar\omega}{dp} = \frac{S_{df}\hbar\omega}{3B}[2(n+1) - 6\gamma] \tag{3}$$

where $\gamma$ is the Grüneisen parameter describing the dependence of phonon energy on crystal compression. Usually the quantity of the exponent $n$ is much smaller than 5 (it is approximately equal to 2–3 (Grinberg 2006)); therefore for an effective Grüneisen parameter greater than unity the quantity $[2(n+1) - 6\gamma]$ can be negative and, according to relation (3), the lattice relaxation energy $S_{df}\hbar\omega$ reduces when pressure increases. The energy of the maximum of the luminescence band related to the $4f^6 5d^1(e_g) \rightarrow {}^8S_{7/2}$ transition $E_{em}$ (arrow 3 in figure 7) is given by the relation

$$E_{em} = E_{df} - 2S_{df}\hbar\omega \tag{4}$$

where $E_{df}$ is the energy of the $4f^6 5d^1(e_g)$ state without lattice relaxation (see figure 7). The effect of pressure on $E_{em}$ is given by the rate

$$\frac{dE_{em}}{dp} = \frac{dE_{df}}{dp} - 2\frac{dS_{df}\hbar\omega}{dp}. \tag{5}$$

Considering figure 7 the difference between the energy of the minimum of the $4f^6 5d^1(e_g)$ electronic configuration and the energy of the ${}^6P_{7/2}$ state $E({}^6P_{7/2})$ is given by

$$\Delta_{df} = E_{df} - S_{df}\hbar\omega - E({}^6P_{7/2}). \tag{6}$$

Since the pressure change of the energy of the ${}^6P_{7/2}$ state, $E({}^6P_{7/2})$, was small

$$\frac{d\Delta_{df}}{dp} \approx \frac{dE_{df}}{dp} - \frac{dS_{df}\hbar\omega}{dp}. \tag{7}$$

Further relations (5) and (7) yield

$$\frac{dE_{em}}{dp} = \frac{d\Delta_{df}}{dp} - \frac{dS_{df}\hbar\omega}{dp}. \tag{8}$$

Pressure reduced significantly the energies $E_{df}$ and then $\Delta_{df}$. However, when pressure caused a reduction of the energy of $S_{df}\hbar\omega$ the change in energy of the $4f^6 5d^1(e_g) \rightarrow {}^8S_{7/2}$ luminescence $E_{em}$ can be very small due to compensation described by relation (8).

The model of the impurity trapped exciton has been analyzed in the papers Gryk *et al* (2005) and Grinberg and Mahlik (2008). Two types of impurity trapped excitons have been considered, depending on if the electron or hole is localized at the impurity. In both cases the second charge (hole or electron, respectively) is attracted by the Coulomb potential of the ionized impurity and occupies so-called Rydberg states. It has been considered by Grinberg and Mahlik (2008) that the energy of the exciton trapped at the impurity can increase or decrease with pressure when one deals with an electron or hole localized at the impurity. The experimentally observed increase of the energy of the trapped exciton with pressure would suggest that we are dealing with a localized electron system. On the other hand, such a system needed the existence of the stable $Eu^{1+}$, which has not been reported so far. On the other hand, it has been shown (Mahlik *et al* 2008, 2009) that in the case of $Ba_{0.5}Sr_{0.5}F_2$:$Eu^{2+}$ and $Ba_{0.3}Sr_{0.7}F_2$:$Eu^{2+}$, where one dealt with the $Eu^{2+}$ trapped exciton with a hole localized at $Eu^{2+}$ ($Eu^{3+}$ + electron attracted by the Coulomb potential), the energy of the impurity trapped exciton can decrease and increase with increasing pressure. The last effect is due to the rapid reduction of the electron–lattice interaction (Mahlik *et al* 2009).

According to these considerations the energy of the $Eu^{2+}$ trapped exciton $E_{ef}$ is given by the energy of the conduction band edge $E_{cb}$ reduced by a quantity related to electron delocalization $\Delta E$:

$$\Delta E = \frac{C}{R^m} \tag{9}$$

and additionally reduced by an energy related to lattice relaxation:

$$S_{ef}\hbar\omega = \frac{k}{2}\Delta^2 = \frac{m^2C^2}{2kR^{2(m+1)}} \tag{10}$$

where

$$\Delta = -\frac{mC}{kR^{m+1}} \tag{11}$$

is the quantity describing the compression of the ligands as the response to decreasing the number of electrons at the europium ion, $R$ is the $Eu^{2+}$–ligand distance. The exponent $m$ depends on the model, $m = 1$ for classic electrostatic potential (Madelung potential), $m = 2$ corresponds to the energy of the electron in a quantum well, $m = 5$ corresponds to the energy of an electron in the crystal field and $m = 12$

corresponds to inter-ionic repulsion given by the Lennard-Jones potential. Actually one has to consider the effective $m$ which is between 2 and 5. The quantity $C$ depends on the probability of finding a 'delocalized' electron in the core region of $Eu^{3+}$ (a distance smaller than $R$). Assuming that the delocalized state is described by the wavefunction $F_{ex}(\mathbf{r})$

$$C = C_0\left(1 - \int_0^R |F_{ex}(\mathbf{r})|^2 \mathrm{d}\mathbf{r}\right) \tag{12}$$

where $C_0$ is related to fundamental constants and integration is over the space between the central ion and ligands.

Relation (9) allowed us to calculate the rates describing the pressure changes of the exciton energy:

$$\frac{\mathrm{d}\Delta E}{\mathrm{d}p} = m\frac{\Delta E}{3B} \tag{13}$$

the electron–lattice interaction energy:

$$\frac{\mathrm{d}S_{\mathrm{ef}}\hbar\omega}{\mathrm{d}p} = \frac{S_{\mathrm{ef}}\hbar\omega}{3B}[2(m+1) - 6\gamma] \tag{14}$$

and the ion shift:

$$\frac{\mathrm{d}\Delta}{\mathrm{d}p} = -\Delta\cdot\left[\frac{1}{k}\frac{\mathrm{d}k}{\mathrm{d}p} + (m+1)\frac{1}{R}\frac{\mathrm{d}R}{\mathrm{d}p}\right] = \frac{\Delta}{3B}\left[(m+1) - 6\gamma\right]. \tag{15}$$

One noticed $\frac{\mathrm{d}\Delta}{\mathrm{d}p} < 0$ when $[(m+1) - 6\gamma] < 0$. It was very possible that pressure reduced the quantity $\Delta$ since the values of the Grüneisen parameter are of the order of unity or greater, see table 1. The shifted ligands created the energy barrier where the height is proportional to $\Delta$, which prevented the electron bounded by the Coulomb potential to penetrate the space near the $Eu^{3+}$ (Mahlik *et al* 2009). When increasing pressure decreased the ligands' shifts $\Delta$ and energy barrier it changed the electron distribution $|F_{ex}(\mathbf{r})|^2$ and reduced the quantity $C$ (see relation (12)). Thus the quantities $\Delta E$ and $S_{\mathrm{ef}}\hbar\omega$ reduced due to the reduction of $\Delta$. As a result the energy $\Delta_{\mathrm{ef}}$ given by relation

$$\Delta_{\mathrm{ef}} = E_{\mathrm{cb}} - \Delta E - S_{\mathrm{ef}}\hbar\omega - E(^6\mathrm{P}_{7/2}) \tag{16}$$

increased with increasing pressure as was detected.

## 5. Conclusions

Our time-resolved spectroscopy measurements and high pressure luminescence measurements allowed us to develop the configurational coordinate diagram representing the energetic structure of the $LiBaF_3:Eu^{2+}$ system, which explained the pressure dependence of the luminescence lineshape and luminescence kinetics.

Disappearance of the broad band luminescence peaked at 24 500 $cm^{-1}$ under pressure evidently excluded the earlier attributions of this emission to the $4f^65d^1(e_g) \rightarrow {}^8S_{7/2}$ transition in $Eu^{2+}$ (Meijerink 1993, Zhou *et al* 2002). The fact that this luminescence had the same decay as the $^6P_{7/2} \rightarrow {}^8S_{7/2}$ luminescence at all considered pressures and temperatures shows that its initial state and the $^6P_{7/2}$ state of $Eu^{2+}$ are in thermal equilibrium. Thus the concept which relates the broad band emission to traces of oxygen in the material (Hua *et al* 2003) was shown to be false. We showed that the $4f^65d^1(e_g) \rightarrow {}^8S_{7/2}$ transition in $LiBaF_3:Eu^{2+}$ can be observed under high hydrostatic pressure as the broad band with maximum intensity at energy 28 000 $cm^{-1}$.

## Acknowledgments

This paper has been supported by the Polish Ministry of Science and Higher Educations through a grant active in the years 2008–2011. One of us (SM) has been supported by the European Social Fund.

## References

Aldshuler N S, Korableva S L, Livanova L D and Stolov A L 1974 *Sov. Phys.—Solid State* **15** 2155
Baldochi S L and Gesland J Y 1992 *Mater. Res. Bull.* **27** 891
Cooke A H, Jones D A, Silva J F A and Weith M R 1975 *J. Phys. C: Solid State Phys.* **8** 4083
Dorenbos P 2000 *J. Lumin.* **91** 155
Dorenbos P 2003a *J. Lumin.* **104** 239
Dorenbos P 2003b *J. Phys.: Condens. Matter* **15** 2645
Ehrilich D J, Moulton P F and Osgood R M 1979 *Opt. Lett.* **4** 184
Eibshultz M, Guggenheim H J, Wemple S H, Camlibel I and Didomenico M 1969 *Phys. Lett.* **7** 409
Gatch D B, Boye D M, Shen Y R, Grinberg M, Yen Y N and Meltzer R S 2006 *Phys. Rev.* B **74** 195117
Grinberg M 2006 *Opt. Mater.* **28** 26
Grinberg M and Mahlik S 2008 *J. Non-Cryst. Solids* **354** 4163
Gryk W, Dyl D, Ryba-Romanowski W and Grinberg M 2005 *J. Phys.: Condens. Matter* **17** 5381
Haussühl S, Leckebusch R and Recker K 1972 *Z. Naturf.* a **27** 1022
Heaton R A and Lin C 1982 *Phys. Rev.* B **25** 3538
Kubicki A A, Bojarski P, Grinberg M, Sadownik M and Kukliński B 2006 *Opt. Commun.* **269** 275
Mahlik S, Kuklinski B, Yen Y M, Meltzer R S and Grinberg M 2008 *J. Lumin.* **128** 715
Mahlik S, Wiśniewski K, Grinberg M and Meltzer R S 2009 *J. Phys.: Condens. Matter* at press
Marsman M, Andriessen J and van Eijk C W E 2000 *Phys. Rev.* B **61** 16477
Meijerink A 1993 *J. Lumin.* **55** 125
Morrison C A 1980 *J. Chem. Phys.* **B 72** 1001
Hua R, Lei B, Xie D and Shi C 2003 *J. Solid State Chem.* **175** 284
Sarakura N 1995 *Opt. Lett.* **20** 294
Sommerdijk J L, Versteegen J M P J and Bril A 1974 *J. Lumin.* **10** 411
Tröster Th, Schweizer S, Secu M and Spaeth J-M 2002 *J. Lumin.* **99** 343
Tunguy B, Merle P, Pezat M and Fouassier C 1974 *Mater. Res. Bull.* **9** 813
Tyner C E and Drickamer H G 1977 *J. Chem. Phys.* **67** 4116
Zhou Y, Wang D, Zhang G and Zhang X 2002 *Chin. J. Lumin.* **23** 393